JOURNAL OF THE KOREAN ASTRONOMICAL SOCIETY
32: 83 ~ 89, 1999

VIJH SURFACE PHOTOMETRY OF NGC 4314

HONG BAE ANN
Department of Earth Sciences, Pusan National University, Pusan 609-735, Korea
E-mail: hbann@cosmos.es.pusan.ac.kr
(Received Sep. 15, 1999; Accepted Oct. 1,1999)

ABSTRACT

We have conducted a V, I, J, and H surface photometry of a barred galaxy NGC 4314 to analyze the morphology and luminosity distribution of the galaxy. By applying a semi two-dimensional profile decomposition method, we derived the luminosity fractions and the scale lengths of the three distinct components, bulge, disk, and bar: $L_b \approx 0.35$, $L_d \approx 0.35$, $L_{bar} \approx 0.30$, $r_e \approx 22''$, $r_0 \approx 50''$, and $a \approx 60''$. The bulge of NGC 4314 seems to be triaxial due to the isophotal twists but its luminosity distribution is well approximated by the $r^{1/4}$-law.

Key words : galaxies : photometry – galaxies : individual (NGC 4314)

I. INTRODUCTION

NGC4314 is an early type barred galaxy whose Hubble type is SBa. The nuclear region of the galaxy shows a peculiar morphology characterized by hot spots and nuclear spiral arms (Sandage 1961; Sandage & Bedke 1994). There have been a lot of photometric and spectroscopic studies to decipher the nature of the peculiar morphology of NGC 4314 (Burbidge & Burbidge 1962; Lynds, Furenlid, & Rubin 1973; Benedict 1980; Wakamatsu & Nishida 1980; Benedict et al. 1992). According to these studies, it has been known that the peculiar nuclear morphology is caused by a nuclear ring that is bluer than the surrounding regions including the nucleus. The blue color of the nuclear ring is due to the presence of young stellar populations that might be formed from the disk material accumulated near the ILRs of the galaxy (Garcia-Barreto et al. 1991; Benedict et al. 1992; Benedict, Smith, & Kenney 1996).

Recent *HST* images and *HST/NICMOS* image of NGC 4314 (Benedict et al. 1993; Mulchaey 1999) clearly show the young stellar clusters and dust lanes in the nuclear region. The nuclear spiral pattern that is apparent from the ground based observations is found to be caused by the dust lanes that partly obscure the nuclear ring. While the morphology and the luminosity distribution of the nuclear region of NGC 4314 have been analyzed in detail (Garcia-Barreto et al. 1991; Benedict et al. 1992, 1993), little is known about the luminosity distributions of the three main components, disk, bulge, and bar, except the effective radius and effective brightness of the bulge component (Benedict et al. 1992).

NGC 4314 is an ideal object to study the interplay between the nuclear morphology and the underlying dynamics of the galaxy. We aimed to determine the fractional luminosities and scale lengths of the three main components, bulge, disk, and bar by profile decomposition. These structural parameters will be used to build mass models of SPH simulations in which gas responses are compared with the nuclear morphology of NGC 4314 in a forthcoming paper (Ann 1999). To do this, we conducted a *VIJH* CCD surface photometry of NGC 4314. In section II, we present the observations and data reduction. The results are described in section III, and a brief summary and conclusions are given in the last section.

II. OBSERVATIONS AND DATA REDUCTION

(a) Observations

The observations of NGC 4314 in V and I bands were made in 1993 February with TEK 1024 CCD (1024 × 1024) attached to the modified Newtonian focus of the 1.8 m Plaskett Telescope of Dominion Astrophysical Observatory (DAO). The gain and readout noise of the system were $2e^{-1}$/ADU and $12e^{-1}$, respectively. The pixel size is 21 μm which gives the image scale of 0.″47/pixel. The images were obtained with Johnson-Cousin V and I filters with exposure times of 300s and 220s, respectively. Bias frames were obtained before and after the observations and the twilight sky was observed for the flat fields. We observed several Landolt (1992) standard stars for the transformation of the instrumental magnitudes to the standard system. The seeing of the night was about 2.″7.

Auxiliary observation of NGC 4314 were conducted in J and H bands with a Ptsb 256 × 256 IR array and the DAO 1.8 m Plaskett Telescope in 1993 April. The pixel size of the IR array is 30 μm which corresponds to 0.″67 on the sky. The readout noise and the dark of the system were $62e^{-1}$ and $7e^{-1}s^{-1}pixel^{-1}$, respectively. We observed the J- and H- band images of NGC 4314 with exposure time of 480s and obtained a large number of bias and dark frames during the observations. We observed the twilight sky and several standard stars of Elias and Frogel (1982) for the flat fields and the calibration of the IR photometry, respec-

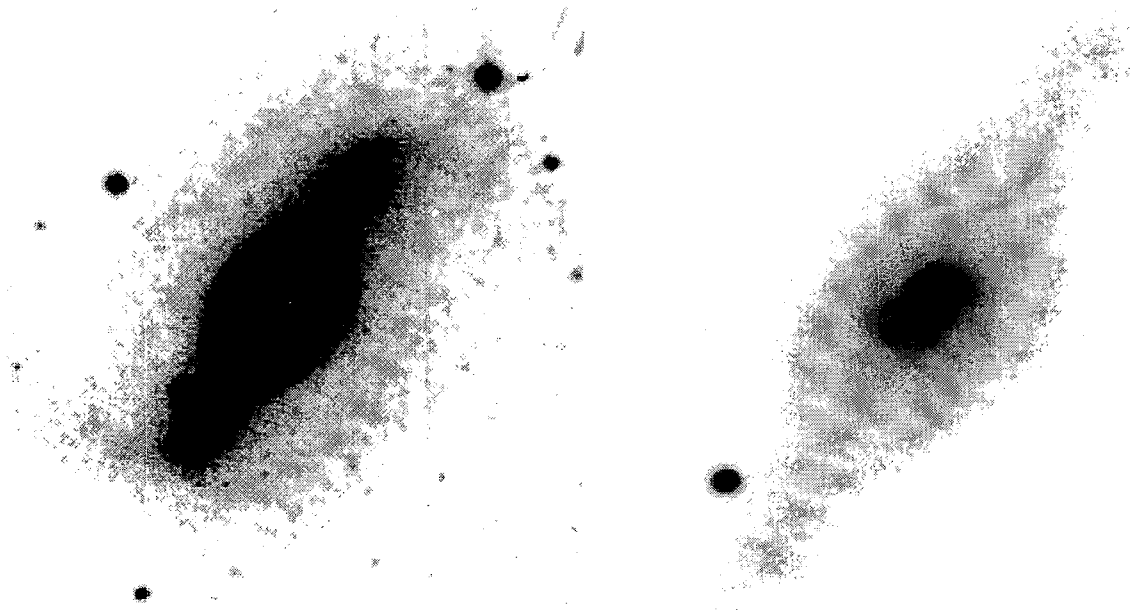

Fig. 1.— Grey scale images of NGC 4314. Right panel shows the central part of the galaxy. North is up and east to the left.

tively. The seeing during the observation was about 3.″6.

(b) Reduction

The basic reductions were carried out using the CCDRED package within IRAF for both the CCD data and the near IR data. This procedure involved bias subtraction with overscan correction, dark subtraction, trimming of the data section, and flat-fielding. We applied dark subtraction to IR data only because it was negligible for CCD frames. The flat fielded frames of the galaxy images were subtracted and divided by the sky frames that were obtained by fitting the sky regions surrounding the galaxy images, by using IRAF/SPIRAL. For the IR data we subtracted a mean sky intensity determined from the pixels near the edges of the IR array because the optical size of the galaxy is comparable to the size of the IR array. Thus, the sky intensity is likely to be somewhat overestimated. However, the errors introduced by the inaccurate estimate of the sky intensity is small because the intensity from the outer region of the galaxy is much lower than the sky intensity. Of course, the morphology of the central part of the galaxy is not much affected by the sky intensity.

III. RESULTS

(a) Morphology

The morphology of NGC 4314 has been described in detail by Benedict et al. (1992), based on *B, V, I, J, H,* and *K* images, The morphological properties described by Benedict et al. (1992) are confirmed by the present photometry. Fig. 1 shows the grey scale images of NGC 4314 in *V*-band. The contrasts are adjusted to see the bar and the outer spiral arms in the left panel and the nuclear structures in the right panel, respectively. The size of the image in the left panel is $3.'5 \times 3.'5$ and that of the right panel is a half of the left panel. As we can see in Fig. 1, the outer spiral arms that emerge from the end of the bar are very faint. The faintness of the outer spiral arms leads to the classification of NGC 4314 as an anemic spiral (van den Bergh 1976). The nuclear ring is displayed as regions of high intensity in the left panel of Fig. 1, which is broken by dust lanes of spiral pattern. There are several hot spots inside the nuclear ring.

The bar of NGC 4314 is very prominent but, as noted by Athanassoula et al. (1990) and Benedict et al. (1992), the length and axial ratio of the bar are difficult to be estimated. Benedict et al. (1992) determined the length and axial ratio of the bar as 66″ and 3, respectively, by fitting a boxy ellipse to the isophote of $\mu_I = 21.5$ mag/arcsec^2. But as evident from the isophotal maps in Fig. 2, the shape of the bar cannot be well represented by ellipses. Thus, we measured the length and axial ratio of the bar by visual inspection of the grey scale images and the isophotal maps. The resulting bar length a and the axial ratio a/b are $a \approx 60''$ and $a/b \approx 4$, respectively. The position angle of the bar is estimated to be about 147°.

As can be seen in Fig. 2, the bulge isophotes are elongated along the bar. It is partly due to the bar luminosity but the intrinsic shape of the bulge of NGC 4314

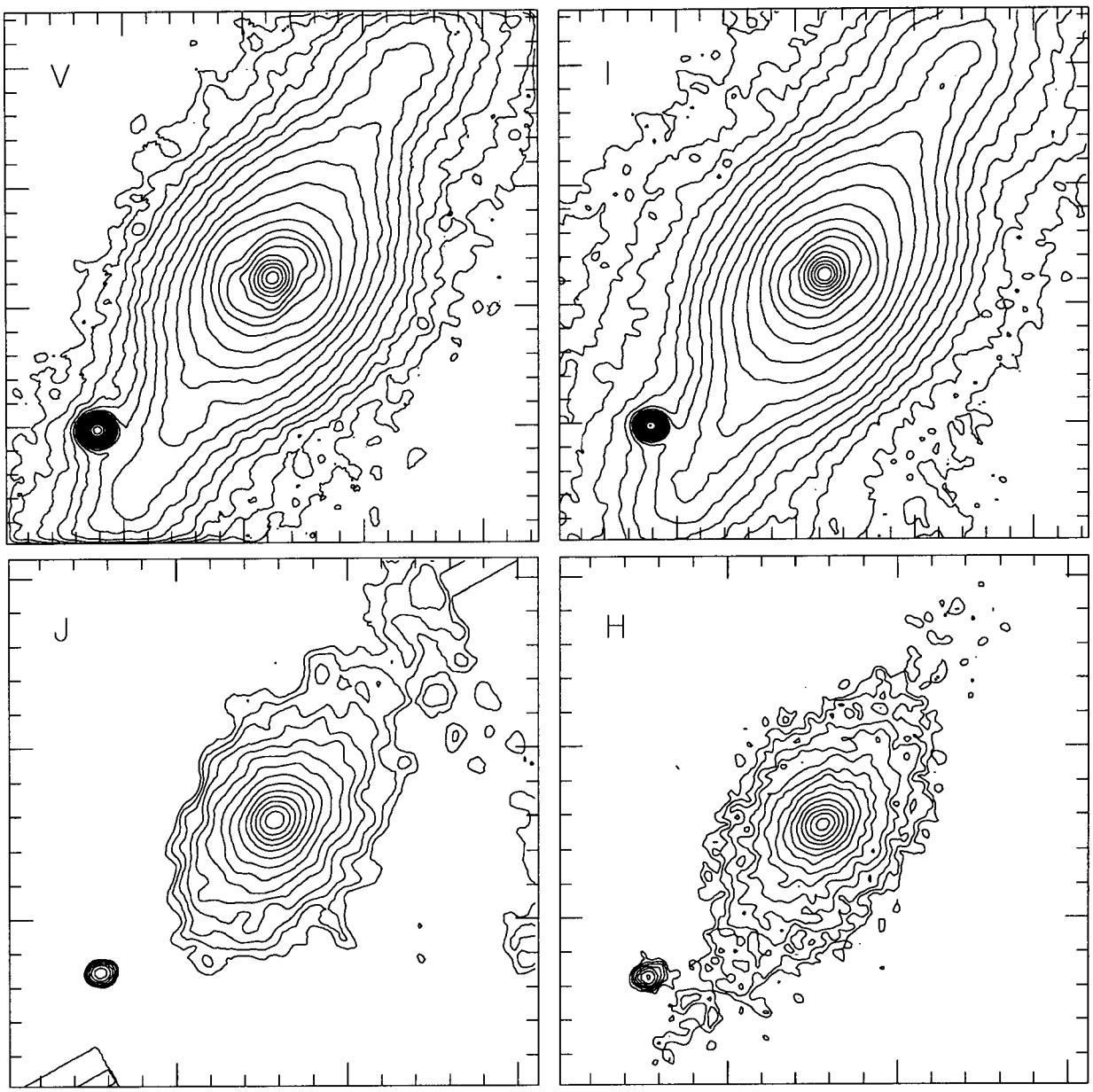

Fig. 2.— Isophotal maps of the central part of NGC 4314. The outer most isophotes are 3 mag/arcsec^2 for V- and I-band images, 5 mag/arcsec^2 for H-band, and 6 mag/arcsec^2 for J-band, respectively. The interval of the isophotes is 0.25 mag/arcsec^2.

might be triaxial with its longest axis aligned parallel to the bar axis. Inside the bulge, there are a nuclear ring and spiral arms which were first discussed by Sandage (1961). Because of the low resolution of our images, the detailed nuclear structures are difficult to be identified. However, features resembling spiral arms are visible in the V-band isophotal map in Fig. 2 but they are disappearing in the J- and H-band maps. The fact that the nuclear spiral pattern is most pronounced in the V-band image with gradual disappearance in the longer effective wavelength suggests the association of the nuclear spiral pattern with the dust lanes. A recent *HST/NICMOS* image of the nuclear region of NGC 4314 (Mulchaey 1999) clearly shows that the nuclear spiral is caused by the dust lanes of spiral pattern that obscure the nuclear ring.

(b) Luminosity Profiles

i) Ellipse fitting

The ellipse fitting technique is effective to derive an average luminosity profile with a high signal-to-noise ratio from a two-dimensional image (Kent 1983). We have applied the ellipse fitting task in IRAF/SPIRAL to the V, I, J, and H images to obtain luminosity profiles as well as profiles of ellipticity (ϵ) and position angle (PA). Fig. 3 shows the profiles of luminosities, ellipticities, and position angles along the major axis of NGC 4314 in V and I bands. We do not present the profiles of J- and H-band images due to the small image sizes and the low signal-to-noise ratios of these images. The ellipticity and position angle profiles of the V- and I-band images are virtually the same and the shapes of the luminosity profiles are similar to each other.

The location of the nuclear ring is easily identified by the shallow gradient of the luminosity profiles and the bump in the ellipticity profiles near $r \sim 8''$. The shallow gradient near $r \sim 8''$ is due to a combined effect of the obscuration by the dust lanes and the luminosity from the nuclear ring. In the bar dominated regions, the luminosity decreases very slowly and the location of the bar end is indicated by an abrupt change of the slope of the luminosity profile and the ellipticity maximum near $r \sim 60''$. The position angle of the bar is about 147° and the ellipticity of the bar is about 0.65 which corresponds to the axial ratio of the major axis length to the minor axis length of the fitted ellipse a/b of 2.86. However, as mentioned in the previous section, the ellipse fit is not a good approximation for the luminosity distribution of the bar of NGC 4314 and the actual bar axial ratio is close to 4.

ii) Radial profiles and bar cross sections

We obtained 72 radial profiles and 17 cross sections across the bar to analyze the luminosity distribution of NGC 4314. The radial profiles are spaced 5° around the galaxy center and the bar cross sections are traced

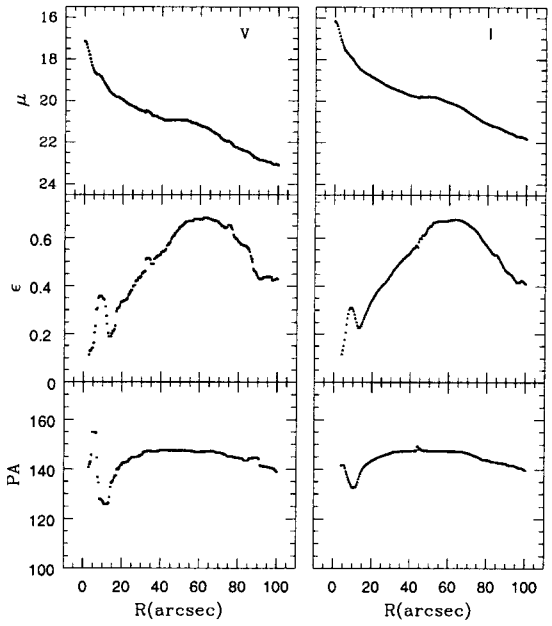

Fig. 3.— Profiles of luminosities, ellipticities, and position angles. For ellipticities and position angles, the data affected by seeing was not plotted.

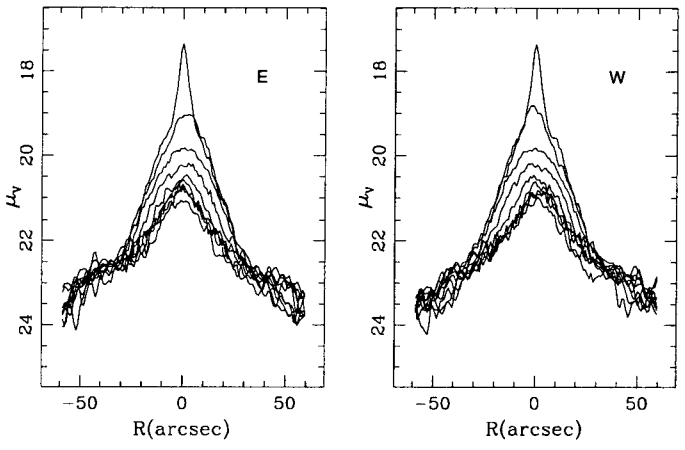

Fig. 4.— Profiles across the bar of NGC 4314. Left panel shows the cross sections in the east side of the bar (E) and right panel for the west side (W).

along the direction perpendicular to the bar major axis with intervals of $\sim 7''$. Fig. 4 shows the measured bar cross sections from the V-band image. The cross sections for the east side of the bar are in the left panel and those for the west side in the right. As we can see in Fig. 4, the shapes of the bar cross sections in the east and west sides of the bar are quite similar, which indicates that the bar luminosity is symmetric in the both sides of the bar. The cross sections near to the center of the galaxy are much affected by the bulge luminosity while the cross sections outside the bulge dominated region ($r > 20''$) have nearly the same shape which is well represented by the Gaussian function. The width of the bar inferred from the bar cross section in $r > 20''$ is about $30''$. These bar cross sections are used to define the Gaussian scale length across the bar in the profile decomposition described below. The brightest cross section in Fig. 4 is the same as the surface brightness profile along the bar minor axis.

(c) Profile Decomposition

i) One-dimensional decomposition

The luminosity profiles of spiral galaxies have been decomposed to the luminosity profiles of the two main components, bulge and disk since the pioneering work of Kormendy (1977). Although there have been several attempts to decompose the luminosity profiles into the bulge and disk components without assuming any specific functions for each component (Kent 1986; Andredakis, Peletier, & Balcells 1995), most profile decomposition methods assume some functional forms. We assumed the $r^{1/4}$-law of de Vaucouleurs (1948) for the bulge component and an exponential function (Freeman 1970) for the disk component. The de Vaucouleurs' law in surface brightness is expressed as

$$\mu(\mathrm{r}) = \mu_{\mathrm{e}} + 8.325[(\mathrm{r}/\mathrm{r_e})^{1/4} - 1] \qquad (1)$$

where μ_e and r_e are the effective brightness and the effective radius of the bulge component, respectively. The exponential function for the disk component is given by

$$\mu(\mathrm{r}) = \mu_0 + 1.086\frac{\mathrm{r}}{\mathrm{r_0}} \qquad (2)$$

where μ_o and r_o are the central surface brightness and the scale length of the disk component, respectively.

For the V- and I-band luminosity profiles along the major axis of NGC 4314, we failed to decompose the observed luminosities into the bulge and disk components by an iterative decomposition method. In the iterative decomposition method, the assumed bulge function is fitted to the observed luminosities in the regions where bulge dominates while the disk fitting function is fitted in the regions where disk dominates. But in the case of NGC 4314, the bar luminosity is too high to be neglected in the regions where the bulge and disk are assumed to be dominant. Thus, as described below, we decomposed the observed luminosity into the three components, bulge, disk, and bar.

However, we decomposed the bulge component from the J- and H-band luminosity profiles along the major axis by assuming that the luminosity from the disk and bar can be approximated by a single exponential function in the central region ($r \leq 30''$). Fig. 5 shows the results of such a decomposition where the $r^{1/4}$-law is assumed for the bulge component and an exponential function is assumed for the luminosity of the disk and bar. As being evident from Fig. 5, the observed luminosity distribution of the central region of NGC 4314 is well approximated by the combination of the $r^{1/4}$-law and an exponential function. There is virtually no difference between the profile decomposition of the J-band image and the H-band image. Because the disk component is much fainter than the bar component in the central region ($r \leq 30''$), the assumed exponential function is thought to represent the luminosity profile of the bar major axis. The good agreement between the model luminosities and the observed ones indicates that the bulge of NGC 4314 is well represented by the classical $r^{1/4}$-law although their morphology is very complicated due to the nuclear ring, hot spots and dust lanes. The derived bulge parameters, $\mu_e(J)$=19.26 (mag/arcsec^2), $r_e(J)$=26″, $\mu_e(H)$=18.38 (mag/arcsec^2), $r_e(J)$=24″, are in a very good agreement with those derived by Benedict et al. (1992) who determined the bulge parameters as $\mu_e(J)$=19.45 (mag/arcsec^2), $r_e(J)$=25″, $\mu_e(H)$=18.71 (mag/arcsec^2), $r_e(J)$=27″, by fitting the $r^{1/4}$-law directly to the observed profiles of the inner region of NGC 4314.

ii) Two-dimensional decomposition

To fully take into account the contribution of the bar luminosity in the decomposition of the observed luminosity of NGC 4314, we decomposed 72 radial profiles and 17 bar cross sections simultaneously into the bulge, the disk, and the bar components. We used the same functional forms for the bulge and the disk (eq. (1) and (2)) as in the one-dimensional decomposition. For the fitting function of the bar component, we adopted an exponential function for the luminosity profile along the bar major axis and the Gaussian function for the bar minor axis that are represented by

$$\mathrm{I(x,y)} = \mathrm{I_{bo}}e^{-(\alpha_1 \mathrm{x} + \beta \mathrm{y}^2)} \quad \text{for } \mathrm{x} \leq \mathrm{a} \qquad (3)$$

$$= \mathrm{I_a}e^{-(\alpha_2(\mathrm{x}-\mathrm{a}) + \beta \mathrm{y}^2)} \quad \text{for } \mathrm{x} > \mathrm{a} \qquad (4)$$

where x and y are rectangular coordinates along and perpendicular to the bar, respectively, and a is the bar radius. I_{bo} and I_a is the central luminosity of the bar and the luminosity at the end of the bar, respectively.

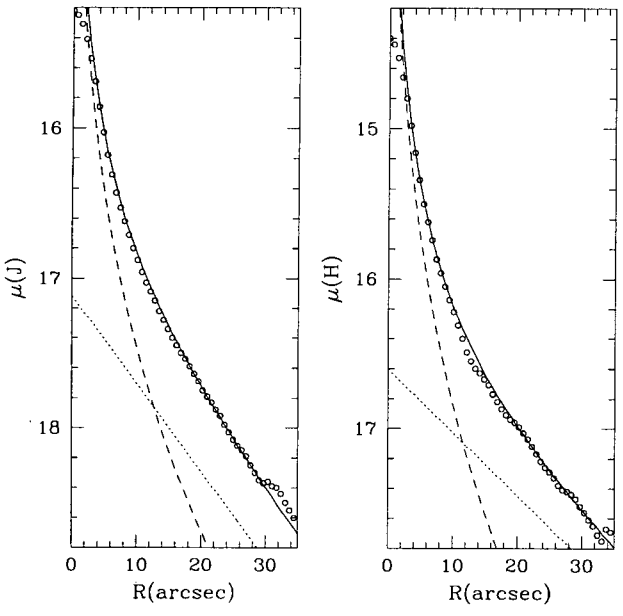

Fig. 5.— Decomposition of elliptically averaged profiles of J and H images. The de Vaucouleurs $r^{1/4}$-law is fitted to the bulge luminosity and an exponential function for the (bar + disk) luminosity.

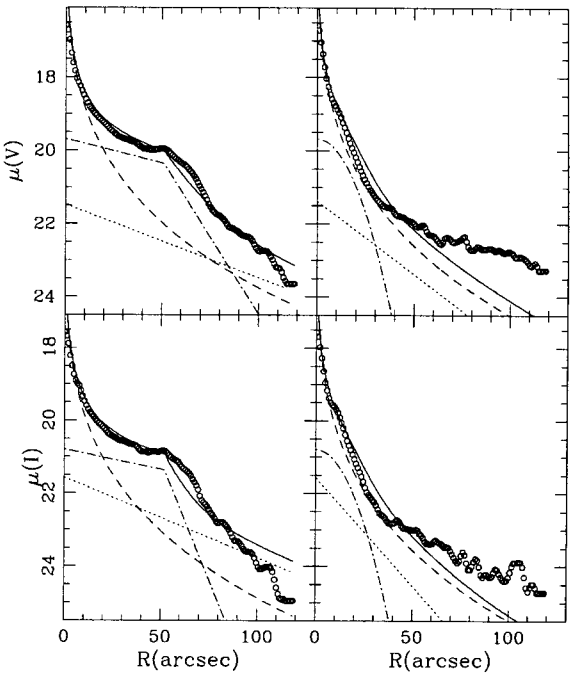

Fig. 6.— Luminosity profiles along the major axis (left panels) and minor axis (right panels) of the bar of NGC 4314. The thin solid lines represent the model profiles that are the sums of the disk (dotted lines), the bar (dot-dashed lines), and the bulge (dashed lines) models, while the open circles indicate the observed luminosities.

The coefficients α_1 and α_2 represent the luminosity gradients along the bar and β is related to the width of the bar. The above functional form for the bar luminosity was introduced by Blackman (1983) and used by Ann & Lee (1987) for a decomposition of the luminosity distribution of 39 barred galaxies.

Our method of profile decomposition is the same as that used by Ann & Lee (1987) which is based on the iterative decomposition technique of Kormendy (1977) but the final check of the fitting is made visually by comparing the model galaxy image built by the decomposed parameters with the observed one on the monitor. In our profile decomposition, the effective brightness of the bulge and the central surface brightness of the disk were used as constraints for the radial profiles in different directions. Our profile decomposition is quite objective but the results of profile decomposition are somewhat dependent on the fitting ranges.

Table 1. Scale parameters and fractional luminosities

Filter	r_e	μ_e	r_0	μ_0	$\frac{L_b}{L}$	$\frac{L_d}{L}$	$\frac{L_{bar}}{L}$
V	21	21.63	40	21.57	0.37	0.32	0.31
I	23	20.87	66	21.38	0.33	0.37	0.30

Fig. 6 shows the results of profile decomposition of the V and I band images where the open circles represent the observed data and the thin solid lines are the combined luminosity profiles of the three components. As shown in Fig. 6, the model profiles fit the major axis profiles quite well while the minor axis profiles show somewhat large discrepancies between the models and the observations. As expected from the luminosity distributions inferred from the gray scale images, the disk component is much fainter than the bar component along the bar major axis. Along the bar minor axis, the luminosity of the bar decreases very rapidly and it is fainter than the disk at $r > 30''$. The bulge dominates the galaxy luminosity in the central region. We list the scale parameters of the bulge and disk in Table 1 along with the fractional luminosities of the main three components, bulge, disk, and bar. The effective radii of the bulge derived from the V-and I-band images are virtually the same but they are slightly smaller than those derived from the one-dimensional decomposition of the J- and H-band profiles. However, this small difference is acceptable if we consider that we did not take into account the disk luminosity properly in the one-dimensional profile decomposition. The large discrepancy between the disk scale lengths derived from

the V- and I-band images is due to the large photometric errors in the luminosities of the outer disk where the disk parameters are derived. The bulge component has about 35% of the total luminosity with the bulge-to-disk ratio L_b/L_d of ~ 1. The fractional luminosity of the bar component L_{bar}/L is estimated to be ~ 0.3. The high fraction of the bar luminosity and the large axial ratio, $a/b \sim 4$, indicate that the bar potential of NGC 4314 is very strong.

IV. A BRIEF SUMMARY AND CONCLUSIONS

We have conducted a *VIJH* surface photometry of a barred galaxy NGC 4314 that has a complicated nuclear morphology. An analysis of the luminosity distribution by means of ellipse fittings to the isophotes and a visual inspection of the isophotal maps and grey scale images show that the bulge of NGC 4314 is triaxial. The complex morphology of the nuclear region is thought to be caused by the hot spots and dust lanes of spiral pattern that obscure the nuclear ring whose location is easily identified by the luminosity and ellipticity profiles.

We derived the scale lengths and the fractional luminosities of the main three components, bulge, disk, and bar, by decomposing the 72 radial profiles and 17 bar cross sections simultaneously. The luminosity profiles of the bulge and disk of NGC 4314 are well approximated by the classical $r^{1/4}$-law and an exponential function, respectively, while the luminosity distributions of the bar are well represented by an exponential function along the bar major axis and the Gaussian function along the bar minor axis.

The luminosity fractions of the three components are comparable to each other with a slightly smaller luminosity of the bar component. However, the bar of NGC 4314 is very strong with its axial ratio of 4 and dominates the luminosity distribution of the inner disk.

The author would like to thank for the hospitality provided by DAO. This work was supported in part by the Basic Science Research Institute Program, Ministry of Education, BSRI-98-5411.

REFERENCES

Andredakis, Y. C., Peletier, R. F., & Balcells, M. 1995, MNRAS, 275, 874

Ann, H. B., & Lee, S.-W. 1987, JKAS, 20, 49

Ann, H. B. 1999, in preparation

Athanassoula, E. 1992, MNRAS, 259, 345

Benedict, G. F. 1980, AJ, 85, 513

Benedict, G. F., Higdon, J. L., Tollestrup, E. V., Hahn, J., and Harvey, P. M. 1992, AJ, 103, 757

Benedict, G. F., Higdon, J. L., Jefererys, W. H., Duncombe, R., Hemenway, P. D, Shelus, P. J., Whipple, A. L., Nelan, E., Stroy, D., Mcarthur, B., & MacCartney, J. 1993, AJ, 105, 1369

Benedict, G. F., Smith, B. J., & Kenney, J. D. 1996, AJ, 111, 1861

Blackman, C. P. 1983, MNRAS, 202, 379

Burbidge, E. M., & Burbidge, G. R. 1962, ApJ, 135, 694

de Vaucouleurs, G. 1948, Ann, d'Astrophys, 11, 487

Elias, J. H., & Frogel, J. A. 1982, AJ, 87, 1029

Garcia-Barreto, J. A., Downes, D., Combes, F., Gerin, M., Megri, C., Carrasco, L., and Cruz-Gonzalez, I. 1991, A&A, 244, 257

Kent, S. M. 1983, ApJ, 266, 562

Kent, S. M. 1986, AJ, 93, 1301

Kormendy, J. 1977, ApJ, 217, 406

Freeman, K. C. 1970, ApJ, 160, 811

Landolt, A. U. 1992, AJ, 104, 340

Lynds, B. T., Furenlid, I., & Rubin, J. 1973, ApJ, 182, 659

Mulchaey, J. 1999, in preparation

Sandage, A. 1961, The Hubble Atlas of Galaxies (Carnegie Institute of Washington, Washington, D.C.), Pub. 618

Sandage, A., & Bedke, J. 1994, The Carnegie Atlas of Galaxies (Carnegie Institute of Washington, Washington, D.C.), Pub. 638

van den Bergh, S. 1976, ApJ, 206, 883

Wakamatsu, K., & Nishida, M. T. 1980, PASJ, 32, 389